




Significantly enhanced ductility of Sn–57Bi–1Ag alloy induced by microstructure modulation from in addition

K. X. Xiao^{1,2}, C. J. Li^{1,2,*} , P. Gao^{1,2}, J. H. Qin³, S. X. Guo³, L. Y. Zhao³, J. T. Zhang³, Q. He³, J. B. Peng^{4,*}, and J. H. Yi^{1,2}

¹ Faculty of Materials Science and Engineering, Kunming University of Science and Technology, Kunming 650093, China

² Yunnan Engineering Research Center of Metallic Powder Materials, Kunming University of Science and Technology, Kunming 650093, China

³ Yunnan Tin New Material Co. LTD of Yunnan Tin Group (Holding) Co., Ltd, Kunming 650501, China

⁴ Yunnan Tin Group (Holding) Co., Ltd, Kunming 650106, China

Received: 6 June 2023

Accepted: 4 July 2023

Published online:

19 July 2023

© The Author(s), under exclusive licence to Springer Science+Business Media, LLC, part of Springer Nature 2023

ABSTRACT

Aiming to solve the intrinsic brittleness of Sn–Bi solder alloy, the effects of In element on the microstructure evolution, mechanical and soldering properties were systematically investigated in Sn–57Bi–1Ag-based alloy. It was found that the addition of In could fragment the reticular Bi-rich phase and increase the content of β -Sn phase in the Sn–(57 – x)Bi–1Ag– x In alloy, which significantly improved the fracture elongation of the In-containing solder alloy. The elongation of Sn–56.0Bi–1Ag–1.0In reached 68.51%, which was 2.3 times that of Sn–57Bi–1Ag (~ 29.68%). What's more, the fracture mechanism of the alloy changes from brittle fracture to mixed ductile-brittle fracture with the addition of In element, implying a significant progress in solving the brittleness problem of Sn–Bi solder alloy. Meanwhile, compared to Sn–57Bi–1Ag, the lower melting point and solidification temperature of the In-containing solder alloys improved the solderability, which enhances the spreading rate of alloy and results in a maximum spreading rate of 72.00% for the Sn–56.0Bi–1Ag–1.0In. This work provides a valuable guidance for industrial production of solder alloys as it simultaneously improved both the solderability and the ductility of Sn–Bi-based alloys.

1 Introduction

Conventional Sn–Pb solders were extensively utilized in electronic packaging due to their excellent comprehensive performance [1]. Since Pb is harmful both to the environment and to human health [2, 3], lead-

free solders such as Sn–Ag–Cu– [4, 5], Sn–Cu– [6], Sn–Zn– [7] [8–10], and Sn–Bi-based [11–14] alloys have received increasing attention from the researchers. However, except for Sn–Bi solder, the further applications of the above-mentioned solders are largely limited due to their high melting points,

Address correspondence to E-mail: lcj@kust.edu.cn; jubopeng@ytc.cn

which may damage the printed circuit boards (PCBs) and electronic components during soldering. Sn–Bi-based solder alloys with low melting temperatures, low thermal expansions, low surface tensions, and higher strengths than Sn–37Pb have been widely utilized in low-temperature electronic packaging [15]. However, the brittleness of the Sn–Bi solder alloys has always been the bottleneck for their application and can extremely deteriorate the reliability of solder joints [16–18].

Currently, the most efficient method to address the brittleness of Sn–Bi solder alloys is alloying. Elements such as Ag [12, 19], Cu [20, 21], Sb [22], Zn [23], In [24, 25], Cr [26], Ni [27], W [28], Co [11, 29], and rare earths (REs) [30] et al. have been added to Sn–Bi-based solder alloys to attempt to promote the comprehensive performance.

Among the alloying elements mentioned above, Ag is excellent in improving the mechanical properties of Sn–Bi-based solder alloys. Shalaby et al. investigated the effects of Ag and In additions on both the mechanical properties and creep resistance of Sn–58Bi solder [31]. The presence of intermetallic compounds, Ag_3Sn and SnIn_{19} , was confirmed in the solder, which effectively improved the creep resistance and mechanical properties of the solder alloy. And the modulus of elasticity increases from 42.72 GPa for Sn–58Bi to 46.15 GPa for ternary alloy Sn–58Bi–2Ag. The influence of Ag addition to Sn–58Bi solder on SnBi/Cu interfacial reaction and the fracture behavior of the aged SnBiAg/Cu solder joints were investigated by Hu et al. [32]. The results revealed that the Ag element in the solder could diffuse into the Cu substrate during the soldering and aging process, forming a Cu–Ag alloy layer adjacent to the joint interface. The Bi segregation was not observed at the aged SnBiAg/Cu interface, and the embrittlement would not occur at the aged SnBiAg/Cu solder joints once the Bi segregation was restrained. Park et al. used Ag-decorated MWCNT to improve the mechanical, electrical, and thermal reliability of Sn–58Bi solder joints [33]. They found that the bonding strength of solder joints using Sn–58Bi–0.05Ag–MWCNTs was 12% higher than those of other solder joints. Moreover, the electrical resistance of the solder joints using Sn–58Bi–0.1Ag–MWCNTs was lower than that of Sn–58Bi solder joint. Yang et al. found that the $\beta\text{-Ag}_3\text{Sn}$ precipitated as a secondary phase and a heterogeneous nucleation substrate when doping Ag into Sn–Bi eutectic alloys [12].

The Sn–Bi–Ag alloy can have improved ultimate tensile strength (UTS) due to the fine grain strengthening and the secondary phase strengthening. Compared to other Ag-doped alloys, the Sn–58Bi–1Ag alloy showed the best UTS (72 MPa) and better elongation (19.3%). In the above-mentioned studies, despite the significant improvement of Sn–Bi-based solder alloys, the elongation of those still lacks in-depth elaboration, i.e., the brittleness problems associated with the high Bi content in those solders still exist and their current elongation levels are not sufficient for the refinement of the electronics industry. Meanwhile, the theoretical studies of the Sn–Bi-based quaternary solder alloy are not systematic enough. In order to promote the further development of the electronic packaging industry, the research of the Sn–Bi quaternary solder alloy is necessary.

Sn–57Bi–1Ag is a commercial ternary solder alloy, but it still meets with the problem of high brittleness. However, In element has been proved to have “softening effect” on solder alloys in previous studies [15, 24, 34]. Therefore, in this work, we intend to use Sn–57Bi–1Ag ternary solder alloy as a substrate and systematically investigate the effect of the In addition on the microstructure evolution, the phase composition, the thermal properties, the wettability, and the mechanical properties of Sn–57Bi–1Ag-based quaternary solder alloy.

2 Experimental

Sn–(57 – x)Bi–1Ag– x In ($x = 0, 0.5, 1.0, 1.5, 2.0, 2.5$ wt%) solder alloys were prepared using Sn, Bi, and In particles and Ag wire with 99.99% purity. All solder alloys were vacuum sealed in quartz tubes, then melted in a 16-channel tube furnace (GSL-1200X-MGI-16) at 800 °C for 2 h. Subsequently, the molten solder alloys were water-cooled and casted into a cylindrical shape. Schematic diagram of sample preparation is shown in Fig. 1.

Thermal properties of all solder alloys were tested in a Differential Scanning Calorimeter (DSC; TA Instruments DSC 25). The whole test process was carried out under nitrogen protection. The heating temperature range was from 100 to 200 °C with a heating rate of 5 °C/min. The cooling temperature range was from 200 to 100 °C with a cooling rate of 5 °C/min. Next, 0.3 g solder pellets were used for

spreading rate test. The flux-covered (Type of flux: RMA223) solder pellets were placed on the copper substrate (Size of Cu Substrate: 30*30*0.3 mm), and then placed together on a heating table (Type of heating table: JF966-1515) and, kept at 180 °C for 10 s and then cooled in air. The solder spreading rate, S_R , was calculated using [35]:

$$S_R = \frac{D - H}{D} \times 100\% \tag{1}$$

where D shows the diameter of the solder pellets (mm) and H represents the height of the solder joint (mm). The spreading rate test meets the relevant requirements of the Chinese electronics industry standards SJ/T 11390-2009.

X-ray diffraction (XRD; Rigaku, MiniFlex600) was used to obtain the phase composition of the solder alloys. Microstructures of the solder alloys and fracture morphologies of the tensile samples were observed by scanning electron microscope (SEM; Tescan vega3). The elemental composition of each phase was determined by energy dispersive spectroscopy (EDS) in SEM. Chemical element distribution of solder alloys was measured by electron probe micro-analysis (EPMA; SHIMADZU, EPMA-1720 Series). In order to quantify the microstructure change, firstly, a region was randomly selected in the microstructure image, and three straight lines were taken in the horizontal and vertical directions of this area, respectively. Then the software was used to manually count the distance between adjacent Bi sheet layers on each straight line, and the average value is the average lamellar spacing of the eutectic phase (L) [15]. Tensile testing was measured at room temperature using an electronic universal testing machine (SHIMADZU, AG-Xplus 50 kN) at room temperature with a strain rate of $1 \times 10^{-3} \text{ s}^{-1}$.

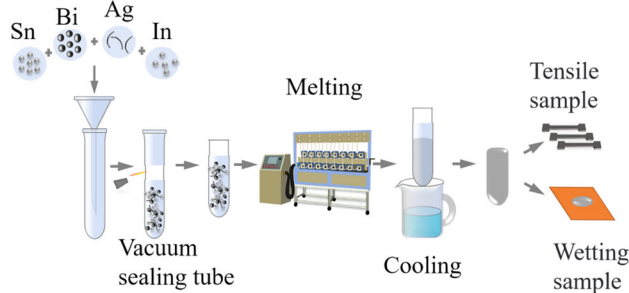


Fig. 1 Schematic diagram of sample preparation

3 Results

3.1 Microstructure evolution

The XRD diffraction pattern of Sn-(57 - x)Bi-1Ag- x In solder alloys are shown in Fig. 2. Three phases, β -Sn, Bi, and Ag_3Sn , are present in the Sn-Bi-Ag solder alloy. However, the low content of Ag_3Sn phase causes the diffraction peaks to be insignificant. After the addition of In, the diffraction peaks of $\text{Ag}_3(\text{Sn}, \text{In})$ appeared in the XRD spectra, and the diffraction intensity became stronger. The SEM images of the Sn-57Bi-1Ag solder alloys with various In contents are displayed in Fig. 3. According to the EDS results (Figs. 4 and 5), all solder alloys contain four different phases, which are the gray β -Sn phase, white Bi-rich phase, dark intermetallic compound and overlapping lamellar Sn-Bi eutectic phase. Combined with the EDS results (Fig. 5) and previous study [36, 37], the dark blocks in the In-containing solder alloys are identified as intermetallic compounds (IMC) whose chemical formula is $\text{Ag}_3(\text{Sn}, \text{In})$. It also can be found that the dark blocks changes from Ag_3Sn into $\text{Ag}_3(\text{Sn}, \text{In})$ in solder alloys when adding In element.

From Fig. 3, the β -Sn phase in the alloys gradually increases with increasing In content and is accompanied by a dendritic to ellipsoidal to strip to ellipsoidal shape transformations. And the continuous reticulated structure of the Bi is disrupted with the addition of In. With the increase of In content, the quantity and size of IMC and the size of Bi-rich phase become larger, and the size of Sn-Bi eutectic phase become smaller. Figure 6 shows the average lamellar spacing of the eutectic phase of Sn-(57 - x)Bi-1Ag- x In solder alloys. With the addition of

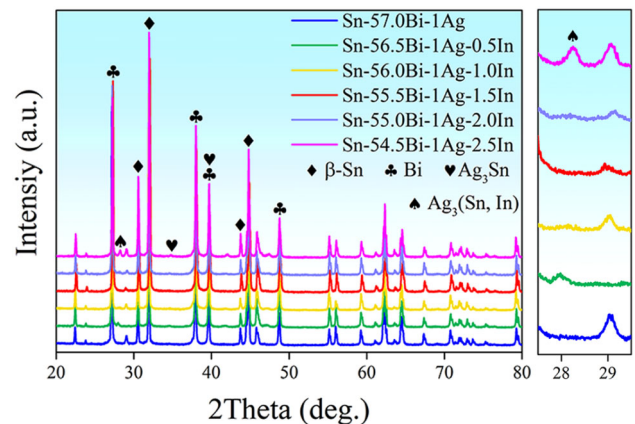


Fig. 2 XRD diffraction pattern of Sn-(57 - x)Bi-1Ag- x In ($x = 0, 0.5, 1.0, 1.5, 2.0, 2.5 \text{ wt}\%$) solder alloys

Fig. 3 Microstructure of Sn–(57 – x)Bi–1Ag– x In solder alloys: **a** $x = 0$ wt%, **b** $x = 0.5$ wt%, **c** $x = 1.0$ wt%, **d** $x = 1.5$ wt%, **e** $x = 2.0$ wt%, **f** $x = 2.5$ wt%

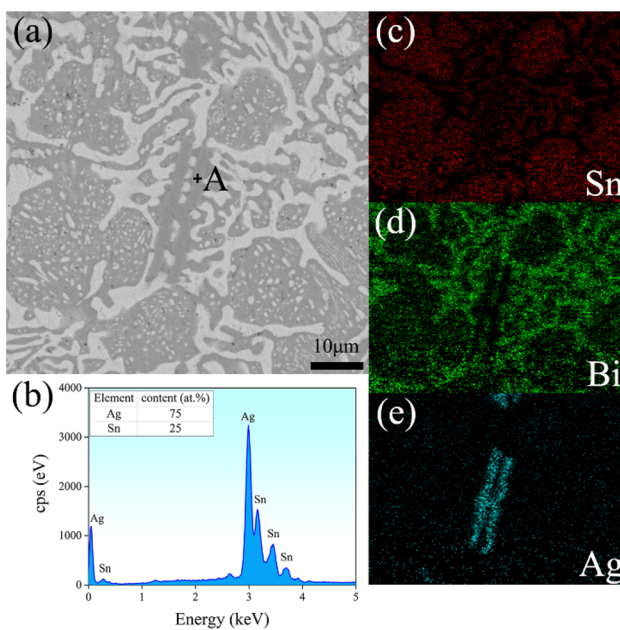
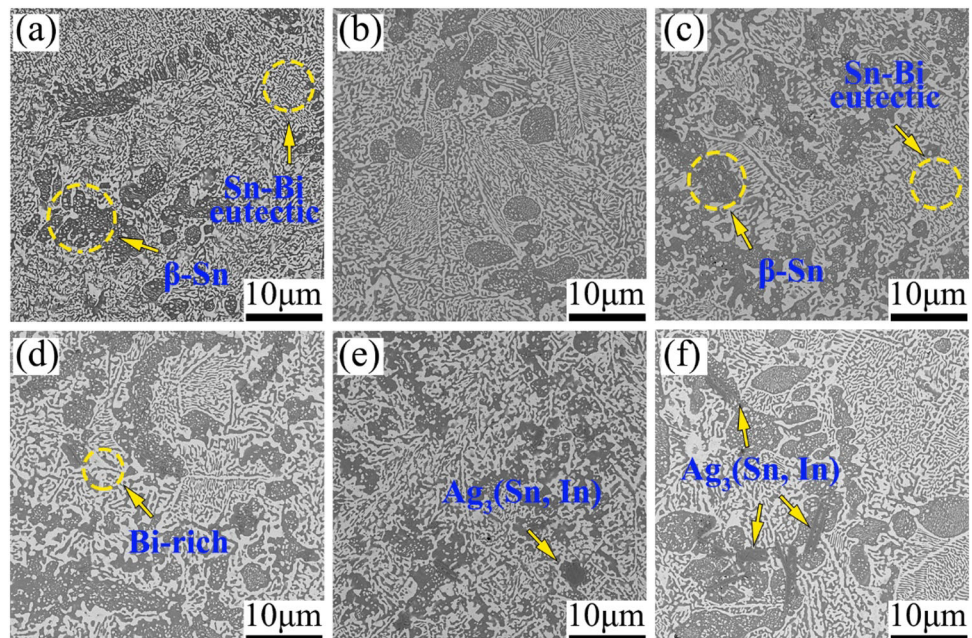


Fig. 4 SEM and EDS results of Sn–57Bi–1Ag: **a** Microstructure of Sn–57Bi–1Ag, **b** Point EDS results in spot A, Mapping EDS results: **c** Sn, **d** Bi, **e** Ag

In, the lamellar spacing of Sn–Bi eutectic phase gradually increases from 2.07 to 3.65 μm .

3.2 Thermal properties

The DSC curves of solder alloys are shown in Fig. 7. All temperature points in Fig. 7 are selected based on

the intersection of the baseline extension and the tangent line at the maximum slope of each peak front as specified by the international confederation for thermal analysis (ICTA). The values of onset temperature ($T_{\text{H-onset}}$ or $T_{\text{C-onset}}$), endset temperature ($T_{\text{H-endset}}$ or $T_{\text{C-endset}}$), and mushy zones range ($\Delta T_{\text{H}} = T_{\text{H-onset}} - T_{\text{H-endset}}$ or $\Delta T_{\text{C}} = T_{\text{C-onset}} - T_{\text{C-endset}}$) of the solder alloys during heating or cooling process, respectively, are listed in Table 1. It is obvious that the $T_{\text{H-onset}}$, $T_{\text{H-endset}}$, $T_{\text{C-onset}}$, and $T_{\text{C-endset}}$ of each solder alloy are decreased with increasing In content. During the heating process, the $T_{\text{H-onset}}$ of solder alloy is decreased from 137.62 to 130.46 $^{\circ}\text{C}$ and the $T_{\text{H-endset}}$ is decreased from 141.34 to 136.30 $^{\circ}\text{C}$. The ΔT_{H} increases slightly from 3.72 to 5.84 $^{\circ}\text{C}$ as the In content increases. During the cooling process, the $T_{\text{C-onset}}$ of solder alloy is decreased from 128.52 to 125.02 $^{\circ}\text{C}$ and the $T_{\text{C-endset}}$ is decreased from 125.21 to 116.76 $^{\circ}\text{C}$. The ΔT_{C} is also increased from 3.31 to 7.98 $^{\circ}\text{C}$.

The $T_{\text{H-onset}}$, $T_{\text{H-endset}}$, $T_{\text{C-onset}}$, $T_{\text{C-endset}}$ of Sn–(57 – x)Bi–1Ag– x In solder alloy is reduced by In addition. The main reason is the solid solution of In elements in Sn which changes the atomic spacing, affecting the bonding force between atoms. And the formation of $\text{Ag}_3(\text{Sn}, \text{In})$ intermetallic compounds will also change the bonding energy of the metal bonds, which reduces the required energy to break the metal bonds during melting. Moreover, metal In is low melting point element and generally the

Fig. 5 SEM and EDS results of Sn–56.0Bi–1Ag–1.0In: **a** SEM image of $Ag_3(Sn, In)$ IMC, **b** Point EDS results for spot B, Mapping EDS results of IMC: **c** Sn, **d** Ag, **e** Bi, **f** In

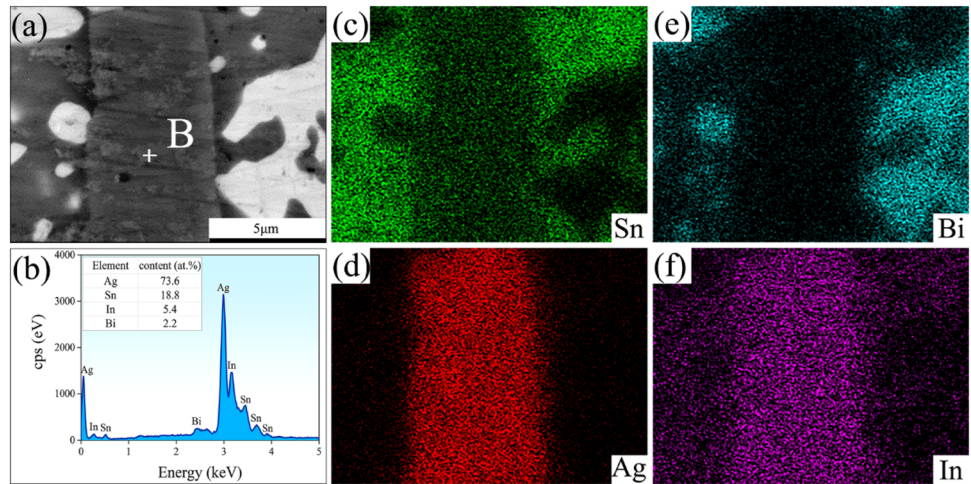


Fig. 6 The average lamellar spacing of the eutectic phase in solder alloys: **a** Measurement spacing diagram, **b** Average lamellar spacing variation curves

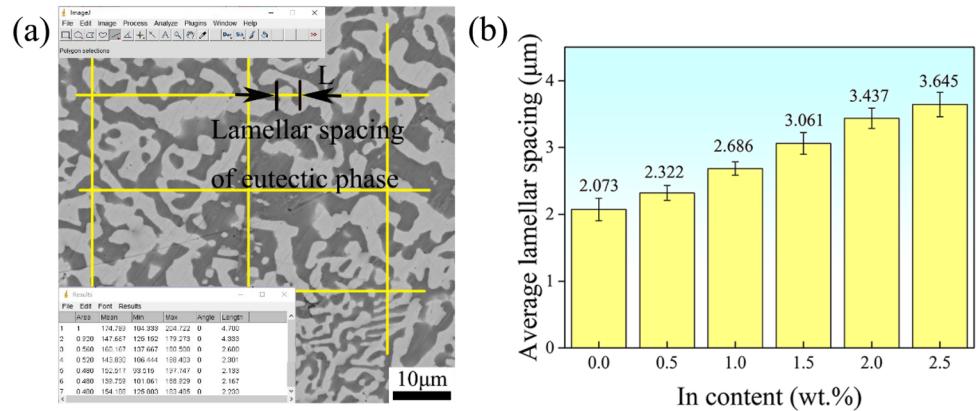
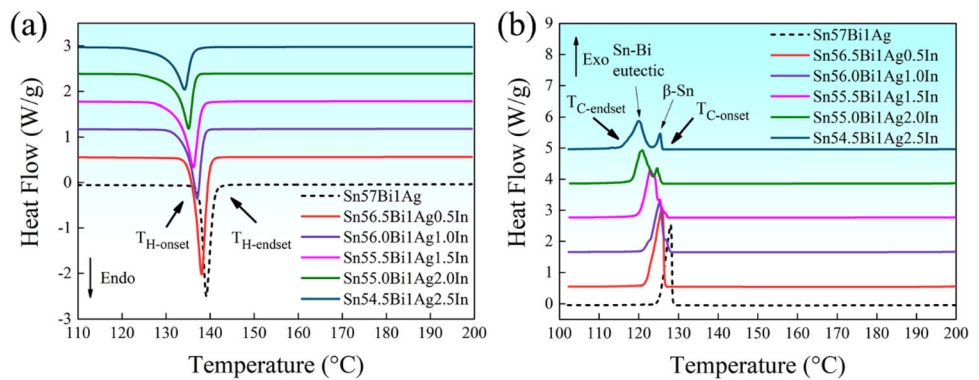


Fig. 7 DSC curves of solder alloys. **a** Heating process, **b** Cooling process



melting point of alloys is lower than that of pure metals, so the melting temperature of In-containing alloy are reduced. Furthermore, the addition of In makes the composition of metal bond in the alloy more complex, requiring a greater span of energy change for the breaking and reorganization of the metal bonds during melting and solidification, which leads to a higher temperature in the mushy zones range (ΔT_H and ΔT_C) of the solder alloy.

What's more, the intensity of Sn–Bi eutectic endothermic peak in Fig. 7a gradually decreases with increasing In content, which indicates that the addition of In can inhibit the formation of Sn–Bi eutectic phase [24]. And this phenomenon is in agreement with the observation of the microstructure (Fig. 3). The narrower mushy zones temperature reflects the shorter coexistence of solid and liquid phases during solidification of the alloy, which ensures reliable joint

Table 1 The values of $T_{H-onset}$, $T_{H-endset}$, $T_{C-onset}$, $T_{C-endset}$ of solder alloys

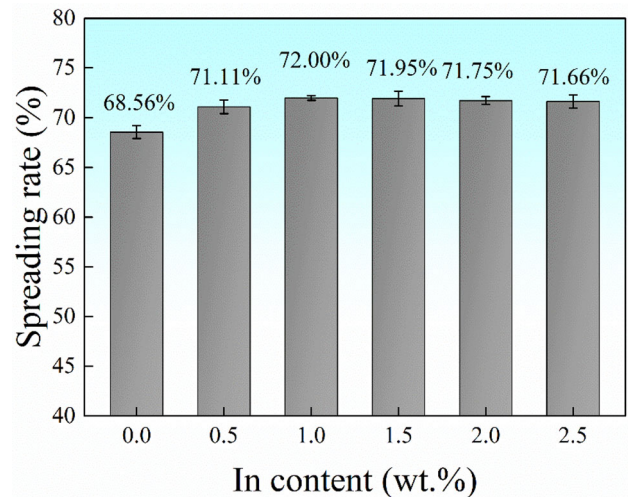
Solder alloys	$T_{H-onset}$ (°C)	$T_{H-endset}$ (°C)	ΔT_H (°C)	$T_{C-onset}$ (°C)	$T_{C-endset}$ (°C)	ΔT_C (°C)
Sn–57Bi–1Ag	137.62	141.34	3.72	128.52	125.21	3.31
Sn–56.5Bi–1Ag–0.5In	135.90	139.71	3.81	126.47	122.44	4.03
Sn–56.0Bi–1Ag–1.0In	134.42	138.72	4.2	125.84	121.22	4.62
Sn–55.5Bi–1Ag–1.5In	132.90	138.24	5.34	125.66	120.26	5.4
Sn–55.0Bi–1Ag–2.0In	132.30	138.09	5.79	125.02	118.42	6.6
Sn–54.5Bi–1Ag–2.5In	130.46	136.30	5.84	125.81	117.83	7.98

formation during the welding process. From Table 1, the mushy zones temperature range for Sn–(57 – x)Bi–1Ag– x In are narrow and all less than 8 °C, indicating that the Sn–(57 – x)Bi–1Ag– x In solder alloy has excellent thermal properties and soldering properties. It is worthy noting that when the In content exceeds 1.5 wt%, there are two exothermic peaks appearing during the solidification process (Fig. 7b). This is because the exothermic peaks of Sn–Bi eutectic phase and β -Sn phase in the Sn–57Bi–1Ag solder alloy are coincide. However, the addition of In increases the β -Sn phase content, which causes the β -Sn phase to release more heat during solidification process. Therefore, there are two exothermic peaks on the exothermic curve.

3.3 Wettability

Wettability of solder alloy is important performance indicator to assess the bonding of the solder joint. And the wettability can be characterized by spreading area, wetting angle, and spreading rate. In present study, the spreading tests are used to measured wettability. The spreading rate results are shown in Fig. 8. It can be found that the spreading rate tends to increase and then decrease with the increase of In content. The spreading rate of Sn–57Bi–1Ag is 68.56%. When 1.0 wt% In is added, the spreading rate of Sn–56.0Bi–1Ag–1.0In increases to a maximum of 72.00%. However, the spreading rate of the solder alloys slightly decreases when the In content is exceeds 1.0 wt%. Nevertheless, the spreading rates of all In-containing solder alloys are improved compared with that of Sn–57Bi–1Ag alloy.

The addition of In element reduces the $T_{H-onset}$ and $T_{H-endset}$ of the solder alloys, which facilitates the increase of the spreading rate. At the same heating temperature, the melt of the solder alloys with lower $T_{H-onset}$ and $T_{H-endset}$ implies a better fluidity, resulting in a higher spreading rate in solder alloy [25].

**Fig. 8** Spreading rate of Sn–(57 – x)Bi–1Ag– x In ($x = 0, 0.5, 1.0, 1.5, 2.0, 2.5$ wt%) solder alloys

Moreover, In is a surface active element, whose addition reduces the surface tension of the molten solder, thus increases the spreading rate of the solder alloy. Also, the addition of In increases the β -Sn phase content, which can increase the contact area between the Sn in the solder alloy and the copper sheet. Therefore, the wetting reaction between the solder alloy and the copper sheet was promoted. However, the decrease in spreading rate when the In content exceeds 1.0 wt% was due to the fact that the generation of IMC reduces the fluidity of the molten solder alloy.

3.4 Mechanical properties

The engineering stress–strain curves, the ultimate tensile strength, and the elongation statistics of Sn–(57 – x)Bi–1Ag– x In solder alloys are shown in Fig. 9. According to Fig. 9b, it is clear that the elongations of Sn–(57 – x)Bi–1Ag– x In solder alloys tends to increase and then decrease with increasing In content. The Sn–56.0Bi–1Ag–1.0In solder alloy shows a substantial

increase of elongation to 68.51%, which is more than 2 times of that of Sn–57Bi–1Ag. Elongation of solder alloy then decreases, dropping to 42.24% at an In content of 2.5 wt%. In addition, the UTS of the Sn–(57 – x)Bi–1Ag– x In solder alloys decreases as the In was added, reaching a minimum strength of 62.83 MPa when 1.5 wt% of In content is added. Nevertheless, the UTS of Sn–(57 – x)Bi–1Ag– x In solder alloy does not change significantly with an increase in In content. The UTS of all In-containing solder alloys exceeded 60 MPa and the elongation was not less than 40%, so the solder alloys exhibited a good balance of UTS and elongation after the addition of In.

Figure 10 shows SEM images of the fracture morphologies of the Sn–57Bi–1Ag, Sn–56.5Bi–1Ag–0.5In, Sn–56.0Bi–1Ag–1.0In, and Sn–55.0Bi–1Ag–2.0In solder alloys. The fracture morphology of the Sn–57Bi–1Ag in Fig. 10a is mostly a smooth and flat cleavage planes, which is mainly produced by the brittle fracture of the massive reticulated Bi phase in the eutectic phase and the bulk Bi-rich phase in the matrix, and there is a small amount of β -Sn phase pulled out in the matrix. Because the deformation ability of the β -Sn phase is better than that of the Bi phase, and the β -Sn phase is fractured after the Bi phase in the tensile process, the fracture morphology of the β -Sn phase shows a “pulled out” state. From Fig. 10b and c, after the In addition, it can be found that the fracture morphologies of the Sn–56.5Bi–1Ag–0.5In and Sn–56.0Bi–1Ag–1.0In solder alloys show less cleavage planes, and the β -Sn phase that is pulled out after large plastic deformation increases significantly with the increase of In content. Therefore, the fracture morphology of the In-containing solder alloys shows the characteristic of unevenness accompanied by voids. Indicating that the fracture mechanism of the solder alloys changes from brittle fracture to mixed ductile-brittle fracture after the

addition of In [12]. Additionally, in Fig. 10c and d, some voids are found on the fracture surface of the solder alloy, the quantity and the size of voids increases with increasing In content. The EDS results of the fracture morphology of Sn–57Bi–1Ag and Sn–56.0Bi–1Ag–1.0In solder alloys are shown in Fig. 11a and b, respectively. From Fig. 11a, the fracture produces a cleavage plane of Bi-phase, while the “drawn-out” structure is the β -Sn phase. In Fig. 11b, some $\text{Ag}_3(\text{Sn}, \text{In})$ IMC fracture generated cleavage planes can also be observed in the voids, which indicates that brittle fracture also occurred in the IMC particles.

4 Discussion

4.1 Microstructure evolution

Schematic diagrams of the solidification growth of solder alloys are shown in Fig. 12. During solidification of the solder alloys, the β -Sn phase nucleates and grows first. As the temperature decreases the eutectic reaction occurs in the alloy melt and the eutectic phase begins to nucleate and grow. At this time, the IMC has two ways of nucleation growth: One is spontaneous nucleation growth, and the other is growth with β -Sn phase and eutectic phase as nucleation substrate [12]. As the Sn–Bi solid solution is a supersaturated solid solution, the Bi-rich phase precipitates in the solder alloys when the temperature drops to room temperature [38]. Finally, the room temperature phase composition of the solder alloys is β -Sn phase + eutectic phase + IMC phase + Bi-rich phase. According to the “similarity-solubility principle,” since Sn and In elements have the same tetragonal crystal structure and similar atomic radius [39], some of the In atoms added to the

Fig. 9 Mechanical properties of Sn–(57 – x)Bi–1Ag– x In solder alloys. **a** Engineering stress–strain curves. **b** Ultimate tensile strength and elongation variation curves

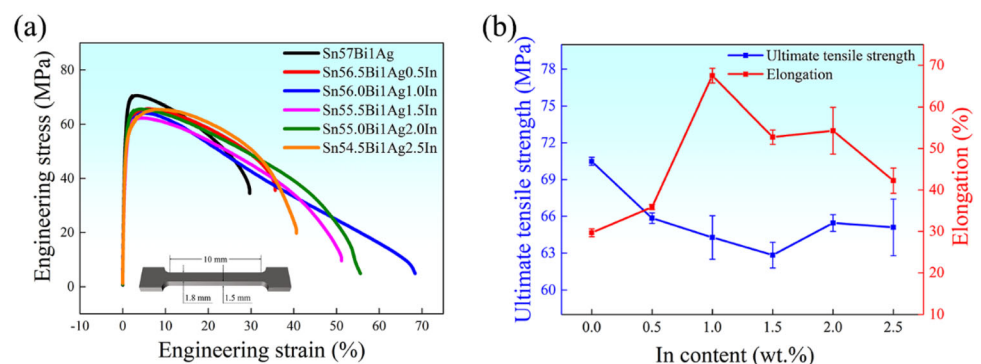


Fig. 10 SEM images of Sn-(57 - x)Bi-1Ag-xIn solder alloys fracture surface. **a** x = 0 wt%, **b** x = 0.5 wt%, **c** x = 1.0 wt%, **d** x = 2.0 wt%

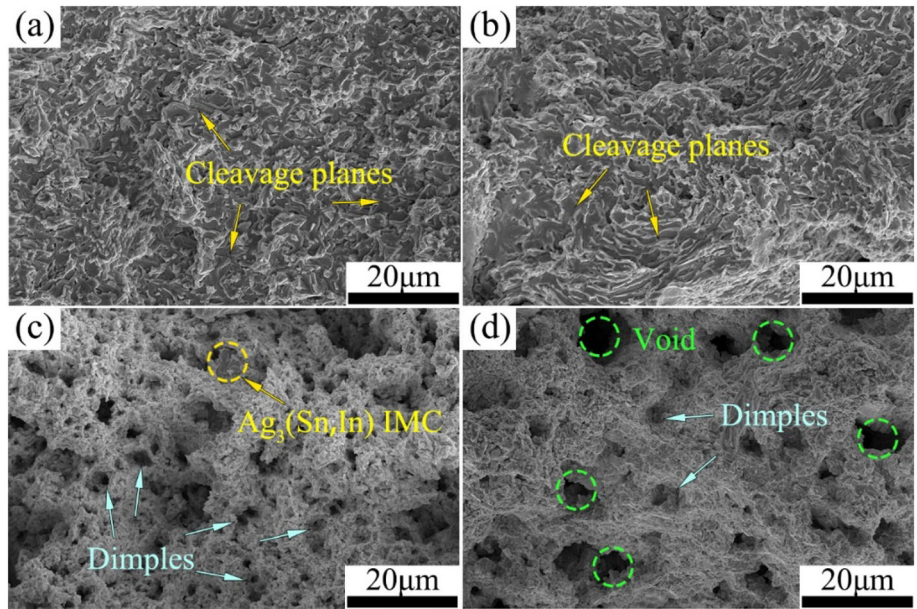


Fig. 11 The fracture morphologies and corresponding EDS results. **a** Sn-57Bi-1Ag, **b** Sn-56.0Bi-1Ag-1.0In solder alloys

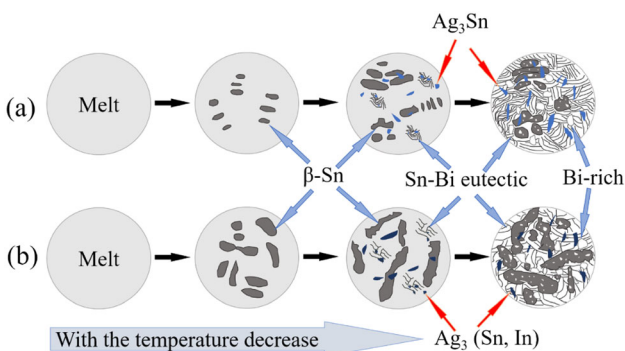
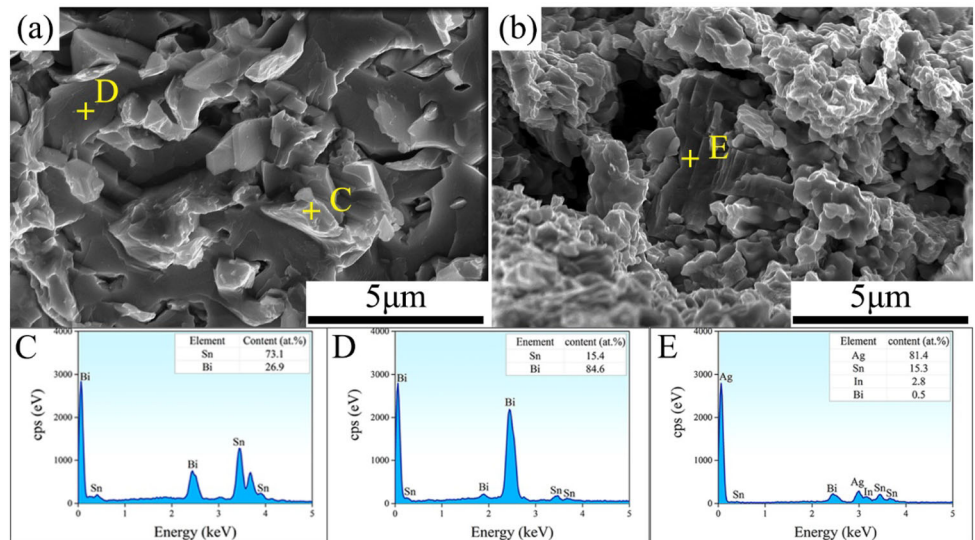


Fig. 12 Schematic diagrams of the solidification growth of the solder alloys. **a** Sn-57Bi-1Ag, **b** Sn-56.0Bi-1Ag-1.0In.

solder alloys are dissolved into the solvent Sn in the form of replacement solid solution. From Fig. 13, the EPMA mapping results of the Sn-56Bi-1Ag-1.0In solder alloy, most of the added In element will be solidly solution in the Sn matrix and some of them will participate in the formation of $Ag_3(Sn, In)$.

Since the eutectic phase is a lamellar structure consisting of Sn and Bi phases, the Bi phase in the eutectic phase forms a continuous reticulation in the solder alloy, and there is also a small amount of Bi-rich phase distributed around the β -Sn phase to make the Bi phase reticulation more continuous. However, when In is added, the temperature range of the

mushy zone increases and more β -Sn phase precipitates in the liquid phase of the alloy so that less of the remaining liquid phase is involved in the eutectic reaction, resulting in a decrease in the amount of eutectic phases generated in the solder alloy. After adding In elements, the mass fraction of Sn atoms in the remaining liquid phase decreases, so the Bi layer in the eutectic phase also becomes thicker. In addition, the coarser growth of the β -Sn phase in the In-containing solder alloy matrix prevents the continuous growth of the eutectic phase, which is separated into smaller eutectic clusters, thus disrupting the continuous reticulation of the Bi phase in the solder alloys. The generation of Bi-rich phase is attributed to the precipitation of more β -Sn phase, which increases the concentration of Bi atoms in the liquid phase of the alloy, resulting in the nucleation and growth of Bi atoms in addition to participating in the eutectic reaction, eventually forming more large Bi-rich phases in the solidified structure of the solder alloy.

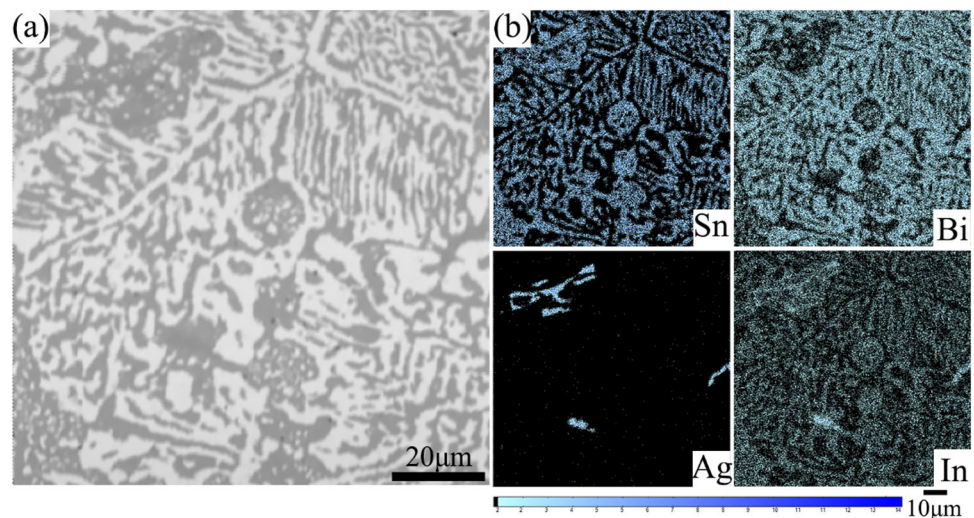
4.2 Ductility enhancement

Since Bi is a brittle phase with poor plastic deformability, the large area of the reticulated Bi phase in the matrix structure of the Sn-57Bi-1Ag solder alloy will be the first to undergo brittle fracture when the reticulated Bi phase is fractured. And the β -Sn phase in the Sn-57Bi-1Ag solder alloy will fracture faster when subjected to larger tensile stresses due to its smaller content and smaller stress area. The fracture mode of Sn-57Bi-1Ag solder alloy is brittle fracture, and the fracture elongation is only 29.68%.

In addition, the fracture of the Sn-57Bi-1Ag solder alloy in Fig. 10a has a large number of cleavage planes, which also proves that the fracture of this solder alloy is brittle fracture. The ultimate tensile strength of Sn-57Bi-1Ag solder alloy is relatively high, reaching 77.64 MPa, due to the small spacing between the layers of its lamellar eutectic structure.

The addition of In element makes the solder alloy free of continuous large eutectic phase, and the β -Sn phase in the alloy increases significantly with the increase of In content. Due to the limited deformation capacity of Bi during the tensile process, the Bi-rich phase will be the first to fracture after the solder alloy yields, and the surrounding eutectic and β -Sn phases will then continue tensile deformation to “wrap” the cleavage plane generated by the fracture of the Bi-rich phase. Therefore, it can be seen from Fig. 10c and d that there are voids in the fracture morphology of the solder alloy due to the fracture of the Bi-rich phase, and there are fewer cleavage planes. However, the fracture morphology of the β -Sn phase indicates that the β -Sn phase is dominated by grain sliding plastic deformation and the fracture mode is ductile fracture. The order of deformability of the various structure in the In-containing solder is: β -Sn phase > eutectic phase > Bi-rich phase and IMC phase. Since more β -Sn phases in the In-containing solder alloys undergo ductile fracture, the fracture morphology of the In-containing solder is characterized by unevenness and accompanied by voids. Therefore, the fracture behavior of the In-containing solder alloys shows mixed ductile-brittle fracture characteristics, and its elongation is higher compared

Fig. 13 EPMA mapping of Sn-56.0Bi-1Ag-1.0In solder alloy. **a** SEM image of Sn-56.0Bi-1Ag-1.0In, **b** EDS mapping results



to that of the Sn–57Bi–1Ag solder alloy, which is consistent with the trend of the elongation of the Sn–(57 – x)Bi–1Ag– x In solder alloy in Fig. 9b, and the fracture elongation of the Sn–56.0Bi–1Ag–1.0In solder alloy is as high as 68.51%.

In Fig. 10c and d, some voids appear on the fracture surface of the solder alloys. This is mainly attribute to the brittle Bi-rich phase and IMC particles which are pulled off first during the tensile process, followed by the β -Sn and eutectic phases continuing to be elongated, and then voids are formed when the solder alloy fractures. As the number of Bi-rich phase and IMC particles increases with the In content, the number of voids on the fracture surface of the In-containing solder alloy tends to increase. When the In content exceeds 1.0 wt%, the elongation of the solder alloy starts to decrease. Combined with the microstructural changes and fracture morphology analysis of the solder alloy, there are three main reasons for this phenomenon: Firstly, the addition of more In elements will lead to the precipitation of larger brittle Bi-rich phase in the solder alloy which will quickly fracture; Secondly, the IMC particles in the solder alloy when subjected to tensile stress will also occur brittle fracture; Lastly, the eutectic phase of the Bi lamellae in the eutectic phase become too thick with increasing In content. These three reasons lead to an increase in the proportion of brittle fracture in the solder alloy during the tensile process, which results in a decreasing trend of the elongation of the solder alloys.

There are two reasons why the addition of In element reduces the strength of the solder alloy: On the one hand, the decrease in the size of the eutectic phase and the increase in the eutectic layer spacing in the In-containing solder alloy lead to a decrease in the ultimate tensile strength of the solder alloy; On the other hand, the addition of In increases the β -Sn phase in the solder alloy, so that the Bi phase is no longer connected to a reticular structure. At this time, the main strength-bearing phase in the solder alloy during tensile deformation is the β -Sn phase, but the strength of the β -Sn phase is lower than that of the reticulated Bi phase, eutectic phase, and IMC phase, so the ultimate tensile strength of the solder alloy decreases after the addition of In. However, the ultimate tensile strength of the solder alloys does not change significantly with increasing In content, mainly because the hard Bi-rich phase and IMC

phase in the solder alloys increase with increasing In content, and the generation of the hard phase counteracts part of the weakening effect of the In element on the ultimate tensile strength of the solder alloy.

5 Conclusion

In this study, the brittleness of the Sn–Bi alloy was solved by In alloying, and the microstructure evolution, phase composition, thermal properties, wettability, and mechanical properties of the solders were systematically investigated and the following main conclusions can be drawn:

1. The Sn–57Bi–1Ag base alloy is composed of β -Sn, Bi-rich, lamellar eutectic, and Ag_3Sn IMC phases. Moreover, the Bi element is distributed in the Bi-rich phase and eutectic phase, forming a continuous reticular structure thus playing as the major origin of the brittleness of the solder.
2. The addition of In can break the reticulated Bi-rich phase to significantly enhance the ductility of solder. The elongation of Sn–56.0Bi–Ag–1.0In alloy reaches 68.51%, which is 2.3 times higher than that of Sn–57Bi–1Ag alloy. The intrinsic brittleness problem of the Sn–Bi-based alloys is well solved.
3. After adding In element, the Ag_3Sn IMC particles transformed into $\text{Ag}_3(\text{Sn}, \text{In})$, and the particle size increased. With increasing In content, β -Sn and Bi-rich phase increase accompanied by the decrease in eutectic phase and fragmentation of the reticulated Bi.
4. Compared to Sn–57Bi–1Ag, 1 wt% In addition reduced the $T_{\text{H-onset}}$, $T_{\text{H-endset}}$, $T_{\text{C-onset}}$, and $T_{\text{C-endset}}$ of the alloy by 7.14 °C, 5.04 °C, 2.51 °C, and 8.45 °C, respectively, which contributes to a 5.02% increase in the spreading rate.

Author contributions

KX: Data curation, Writing—original draft. CL: Writing—review & editing. PG: Methodology. JQ: Resources. SG: Conceptualization. LZ: Investigation. JZ: Supervision. QH: Visualization. JP: Validation. JY: Project administration.

Funding

The authors would like to thank the financial supports of the Science and Technology Major Project of Yunnan Province (Grant No. 2019ZE001-3, 202202AB080001), the National Natural Science Foundation of China (Grant No. 52061021), and the Young and middle-aged academic and technical leaders reserve talent project of Yunnan Province (Grant No. 202005AC160039).

Data availability

The data used to support the findings of this study are included within the article.

Declarations

Competing interests The authors declare that they have no known competing financial interests or personal relationships that could have appeared to influence the work reported in this paper.

Ethical approval This article does not contain any studies involving humans and animals performed by any of the authors.

References

1. C.J. Lee, K.D. Min, H.J. Park, S.-B. Jung, Mechanical properties of Sn-58 wt% Bi solder containing Ag-decorated MWCNT with thermal aging tests. *J. Alloys Compd.* **820**, 153077 (2020). <https://doi.org/10.1016/j.jallcom.2019.153077>
2. Y.-W. Yen, P.-H. Tsai, Y.-K. Fang, S.-C. Lo, Y.-P. Hsieh, C. Lee, Interfacial reactions on Pb-free solders with Au/Pd/Ni/Cu multilayer substrates. *J. Alloys Compd.* **503**, 25–30 (2010). <https://doi.org/10.1016/j.jallcom.2010.04.241>
3. J.W. Yoon, S.W. Kim, S.B. Jung, Interfacial reaction and mechanical properties of eutectic Sn-0.7Cu/Ni BGA solder joints during isothermal long-term aging. *J. Alloys Compd.* **391**, 82–89 (2005). <https://doi.org/10.1016/j.jallcom.2004.09.001>
4. M. Mueller, S. Schindler, K.-J. Wolter, S. Wiese, I. Panchenko, Determination of melting and solidification temperatures of Sn-Ag-Cu solder spheres by infrared thermography. *Thermochim. Acta* **714**, 179245 (2022). <https://doi.org/10.1016/j.tca.2022.179245>
5. R.-D. Wang, Q. Hu, S.-M. Zhang, F.-W. Zhang, C.-T. Lu, Z.-G. Wang, Properties of (Fe-B)-doped Sn-1.0Ag-0.5Cu solders prepared by mechanical alloying. *Rare Met.* **38**, 665–674 (2019). <https://doi.org/10.1007/s12598-019-01248-9>
6. L. Sun, M.H. Chen, L. Zhang, Microstructure evolution and grain orientation of IMC in Cu-Sn TLP bonding solder joints. *J. Alloys Compd.* **786**, 677–687 (2019). <https://doi.org/10.1016/j.jallcom.2019.01.384>
7. F. Li, C. Pu, C. Li, J. Yang, Y. Jia, C. Geng, X. Zhang, Q. Bao, S. Guo, J. Yi, J. Zhang, Study on the effects of Ag addition on the mechanical properties and oxidation resistance of Sn-Zn lead-free solder alloy by high-throughput method. *J. Mater. Sci.: Mater. Electron.* (2023). <https://doi.org/10.1007/s10854-022-09756-8>
8. F. Wang, X. Wang, Z. Lv, C. Hang, H. Chen, M. Li, A novel antioxidant and low-temperature Sn-Zn solder paste based on Zn@Sn core-shell structure. *Mater. Today Commun.* **31**, 103356 (2022). <https://doi.org/10.1016/j.mtcomm.2022.103356>
9. C. Geng, Y. Jia, X. Ma, Y. Jia, Y. Mu, G. Wang, C. Li, J. Peng, Q. Bao, Mechanical properties and oxidation resistance of Sn-Zn-xCu ($2.3 \leq x \leq 20.2$) solder alloys prepared by high-throughput strategy. *Manuf. Lett.* **27**, 47–52 (2021). <https://doi.org/10.1016/j.mfglet.2020.11.005>
10. J.C. Liu, G. Zhang, Z.H. Wang, J.S. Ma, K. Suganuma, Thermal property, wettability and interfacial characterization of novel Sn-Zn-Bi-In alloys as low-temperature lead-free solders. *Mater. Des.* **84**, 331–339 (2015). <https://doi.org/10.1016/j.matdes.2015.06.148>
11. J.X. Hu, N. Su, X.M. Wang, F.C. Yin, X.M. Ouyang, Experimental investigation and thermodynamic calculation of the Co-Sn-Bi ternary system. *CALPHAD* **77**, 102404 (2022). <https://doi.org/10.1016/j.calphad.2022.102404>
12. T. Yang, X. Zhao, Z. Xiong, W. Tan, Y. Wei, C. Tan, X. Yu, Y. Wang, Improvement of microstructure and tensile properties of Sn-Bi-Ag alloy by heterogeneous nucleation of β -Sn on Ag₃Sn. *Mater. Sci. Eng. A* **785**, 139372 (2020). <https://doi.org/10.1016/j.msea.2020.139372>
13. Y. Liu, K.N. Tu, Low melting point solders based on Sn, Bi, and In elements. *Mater. Today Adv.* **8**, 100115 (2020). <https://doi.org/10.1016/j.mtadv.2020.100115>
14. F. Wang, H. Chen, Y. Huang, L. Liu, Z. Zhang, Recent progress on the development of Sn-Bi based low-temperature Pb-free solders. *J. Mater. Sci. Mater. Electron.* **30**, 3222–3243 (2019). <https://doi.org/10.1007/s10854-019-00701-w>
15. Y. Hirata, C.-. Yang, S.-. Lin, H. Nishikawa, Improvements in mechanical properties of Sn-Bi alloys with addition of Zn and In. *Mater. Sci. Eng. A* **813**, 141131 (2021). <https://doi.org/10.1016/j.msea.2021.141131>

16. S.T. Oh, J.H. Lee, Microstructural, wetting, and mechanical characteristics of Sn–57.6Bi–0.4Ag alloys doped with metal–organic compounds. *Electron. Mater. Lett.* **10**, 473–478 (2014). <https://doi.org/10.1007/s13391-014-8002-x>
17. Y.Y. Shiue, T.H. Chuang, Effect of La addition on the interfacial intermetallics and bonding strengths of Sn–58Bi solder joints with Au/Ni/Cu pads. *J. Alloys Compd.* **491**, 610–617 (2010). <https://doi.org/10.1016/j.jallcom.2009.11.017>
18. H.R. Kotadia, P.D. Howes, S.H. Mannan, A review: on the development of low melting temperature Pb-free solders. *Microelectron. Reliab.* **54**, 1253–1273 (2014). <https://doi.org/10.1016/j.microrel.2014.02.025>
19. B.L. Silva, M.G.C. Xavier, A. Garcia, J.E. Spinelli, Cu and Ag additions affecting the solidification microstructure and tensile properties of Sn–Bi lead-free solder alloys. *Mater. Sci. Eng. A* **705**, 325–334 (2017). <https://doi.org/10.1016/j.msea.2017.08.059>
20. C. Peng, J. Shen, W. Xie, J. Chen, C. Wu, X. Wang, Influence of minor Ag nano-particles additions on the microstructure of Sn30Bi0.5Cu solder reacted with a Cu substrate. *J. Mater. Sci. Mater. Electron.* **22**, 797–806 (2010). <https://doi.org/10.1007/s10854-010-0214-8>
21. B.-S. Xu, L.-K. Zang, Z.-F. Yuan, Y. Wu, Z. Zhou, Dissolutive wetting process and interfacial characteristic of molten Sn–17Bi–0.5Cu alloy on copper substrate. *Rare Met.* **32**, 537–543 (2013). <https://doi.org/10.1007/s12598-013-0167-1>
22. J.L. Paixão, L.F. Gomes, R.V. Reyes, A. Garcia, J.E. Spinelli, B.L. Silva, Microstructure characterization and tensile properties of directionally solidified Sn-52 wt% Bi-1 wt% sb and Sn-52 wt% Bi-2 wt% sb alloys. *Mater. Charact.* **166**, 110445 (2020). <https://doi.org/10.1016/j.matchar.2020.110445>
23. J. Shen, Y.Y. Pu, H.G. Yin, Q. Tang, Effects of Cu, Zn on the wettability and shear mechanical properties of Sn–Bi-based lead-free solders. *J. Electron. Mater.* **44**, 532–541 (2014). <https://doi.org/10.1007/s11664-014-3460-3>
24. X. Chen, F. Xue, J. Zhou, Y. Yao, Effect of in on microstructure, thermodynamic characteristic and mechanical properties of Sn–Bi based lead-free solder. *J. Alloys Compd.* **633**, 377–383 (2015). <https://doi.org/10.1016/j.jallcom.2015.01.219>
25. Q. Li, N. Ma, Y. Lei, J. Lin, H. Fu, J. Gu, Characterization of low-melting-point Sn–Bi–In lead-free solders. *J. Electron. Mater.* **45**, 5800–5810 (2016). <https://doi.org/10.1007/s11664-016-4366-z>
26. W. Zhu, W. Zhang, W. Zhou, P. Wu, Improved microstructure and mechanical properties for SnBi solder alloy by addition of Cr powders. *J. Alloys Compd.* **789**, 805–813 (2019). <https://doi.org/10.1016/j.jallcom.2019.03.027>
27. L. Yang, W. Zhou, Y. Ma, X. Li, Y. Liang, W. Cui, P. Wu, Effects of Ni addition on mechanical properties of Sn58Bi solder alloy during solid-state aging. *Mater. Sci. Eng. A* **667**, 368–375 (2016). <https://doi.org/10.1016/j.msea.2016.05.015>
28. Y. Li, K. Luo, A.B.Y. Lim, Z. Chen, F. Wu, Y.C. Chan, Improving the mechanical performance of Sn57.6Bi0.4Ag solder joints on Au/Ni/Cu pads during aging and electromigration through the addition of tungsten (W) nanoparticle reinforcement. *Mater. Sci. Eng. A* **669**, 291–303 (2016). <https://doi.org/10.1016/j.msea.2016.05.092>
29. Y.-C. Huang, S.-W. Chen, Effects of Co alloying and size on solidification and interfacial reactions in Sn-57 wt.%Bi–(Co)/Cu couples. *J. Electron. Mater.* **40**, 62–70 (2010). <https://doi.org/10.1007/s11664-010-1386-y>
30. J. Shen, C. Wu, S. Li, Effects of rare earth additions on the microstructural evolution and microhardness of Sn30Bi0.5Cu and Sn35Bi1Ag solder alloys. *J. Mater. Sci. Mater. Electron.* **23**, 156–163 (2011). <https://doi.org/10.1007/s10854-011-0566-8>
31. R.M. Shalaby, Effect of silver and indium addition on mechanical properties and indentation creep behavior of rapidly solidified Bi–Sn based lead-free solder alloys. *Mater. Sci. Eng. A* **560**, 86–95 (2013). <https://doi.org/10.1016/j.msea.2012.09.038>
32. F.Q. Hu, Q.K. Zhang, J.J. Jiang, Z.L. Song, Influences of Ag addition to Sn–58Bi solder on SnBi/Cu interfacial reaction. *Mater. Lett.* **214**, 142–145 (2018). <https://doi.org/10.1016/j.matlet.2017.11.127>
33. B.-G. Park, W.-R. Myung, C.-J. Lee, S.-B. Jung, Mechanical, electrical, and thermal reliability of Sn–58 wt%Bi solder joints with Ag-decorated MWCNT for LED package component during aging treatment. *Compos. B Eng.* (2020). <https://doi.org/10.1016/j.compositesb.2019.107617>
34. R.K. SHIUE, L.W. TSAY, C.L.L. LIN, J.L. OU, A study of Sn–Bi–Ag–(In) lead-free solders. *J. Mater. Sci.* **38**, 1269–1279 (2003). <https://doi.org/10.1023/A:1022822127193>
35. N. Jiang, L. Zhang, L.L. Gao, X.G. Song, H. Peng, Recent advances on SnBi low-temperature solder for electronic interconnections. *J. Mater. Sci. Mater. Electron.* **32**, 22731–22759 (2021). <https://doi.org/10.1007/s10854-021-06820-7>
36. Y.Y. Chiang, R. Cheng, A.T. Wu, Effects on undercooling and interfacial reactions with Cu substrates of adding Bi and in to Sn–3Ag solder. *J. Electron. Mater.* **39**, 2397–2402 (2010). <https://doi.org/10.1007/s11664-010-1347-5>
37. Z.H. Zhou, Y.C. Liu, M.J. Dong, Z.M. Gao, H.J. Li, Microstructure and interface evolution of Sn–2.5Bi–1.4In–1Zn–0.3Ag/Cu joint during isothermal aging. *J. Mater. Sci. Mater. Electron.* **24**, 4122–4128 (2013). <https://doi.org/10.1007/s10854-013-1370-4>

38. R.T.J.I. Kivilahti, *International symposium on advanced packaging materials* (1998), p. 170–174
39. S.K. SEO, M.G. CHO, H.M. LEE, W.K. CHOI, Comparison of Sn_{2.8}Ag₂₀In and Sn₁₀Bi₁₀In solders for intermediate-step soldering. *J. Electron. Mater.* **35**, 1975–1981 (2006). <https://doi.org/10.1007/s11664-006-0302-y>

Publisher's Note Springer Nature remains neutral with regard to jurisdictional claims in published maps and institutional affiliations.

Springer Nature or its licensor (e.g. a society or other partner) holds exclusive rights to this article under a publishing agreement with the author(s) or other rightsholder(s); author self-archiving of the accepted manuscript version of this article is solely governed by the terms of such publishing agreement and applicable law.